Molecular Imaging and Biology (2024) 26:858–868
https://doi.org/10.1007/s11307-024-01948-4

RESEARCH ARTICLE

Development of ^{52}Mn Labeled Trastuzumab for Extended Time Point PET Imaging of HER2

James M. Omweri[1,2] · Shefali Saini[1,2] · Hailey A. Houson[2] · Volkan Tekin[2] · Jennifer M. Pyles[1,2] · Candace C. Parker[1,2] · Suzanne E. Lapi[1,2]

Received: 6 May 2024 / Revised: 16 August 2024 / Accepted: 19 August 2024 / Published online: 27 August 2024
© The Author(s) 2024

Abstract

Purpose Due to their long circulation time in the blood, monoclonal antibodies (mAbs) such as trastuzumab, are usually radiolabeled with long-lived positron emitters for the development of agents for Positron Emission Tomography (PET) imaging. Manganese-52 (^{52}Mn, $t_{1/2}=5.6$ d, $\beta^+=29.6\%$, $E(\beta_{ave})=242$ keV) is suitable for imaging at longer time points providing a complementary technique to Zirconium-89 (^{89}Zr, $t_{1/2}=3.3$ d, $\beta^+=22.7\%$, $E(\beta_{ave})=396$ keV)) because of its long half-life and low positron energy. To exploit these properties, we aimed to investigate suitable bifunctional chelators that could be readily conjugated to antibodies and labeled with ^{52}Mn under mild conditions using trastuzumab as a proof-of-concept.

Procedures Trastuzumab was incubated with S-2-(4-isothiocyanatobenzyl)-1,4,7,10-tetraazacyclododecane tetraacetic acid (p-SCN-Bn-DOTA), 1-Oxa-4,7,10-tetraazacyclododecane-5-S-(4-isothiocyantobenzyl)-4,7,10-triacetic acid (p-SCN-Bn-Oxo-DO3A), and 3,6,9,15-tetraazabicyclo[9.3.1] pentadeca-1(15),11,13-triene-4-S-(4-isothiocyanatobenzyl)-3,6,9-triacetic acid (p-SCN-Bn-PCTA) at a tenfold molar excess. The immunoconjugates were purified, combined with [^{52}Mn]$MnCl_2$ at different ratios, and the labeling efficiency was assessed by iTLC. The immunoreactive fraction of the radiocomplex was determined through a Lindmo assay. Cell studies were conducted in HER2 + (BT474) and HER2- (MDA-MB-468) cell lines followed by *in vivo* studies.

Results Trastuzumab-Oxo-DO3A was labeled within 30 min at 37 °C with a radiochemical yield (RCY) of 90 ± 1.5% and with the highest specific activity of the chelators investigated of 16.64 MBq/nmol. The labeled compound was purified with a resulting radiochemical purity of > 98% and retained a 67 ± 1.2% immunoreactivity. DOTA and PCTA immunoconjugates resulted in < 50 ± 2.5% (RCY) with similar specific activity. Mouse serum stability studies of [^{52}Mn]Mn-Oxo-DO3A-trastuzumab showed 95% intact complex for over 5 days. Cell uptake studies showed higher uptake in HER2 + (12.51 ± 0.83% /mg) cells compared to HER2- (0.85 ± 0.10%/mg) cells. PET images of mice bearing BT474 tumors showed high tumor uptake that was consistent with the biodistribution (42.02 ± 2.16%ID/g, 14 d) compared to MDA-MB-468 tumors (2.20 ± 0.80%ID/g, 14 d). Additionally, both models exhibited low bone uptake of < 1% ID/g.

Conclusion The bifunctional chelator p-SCN-Bn-Oxo-DO3A is promising for the development of ^{52}Mn radiopharmaceuticals as it was easily conjugated, radiolabeled at mild conditions, and illustrated stability for a prolonged duration both *in vitro* and *in vivo*. High-quality PET/CT images of [^{52}Mn]Mn-Oxo-DO3A-trastuzumab were obtained 14 d post-injection. This study illustrates the potential of [^{52}Mn]Mn-Oxo-DO3A for the evaluation of antibodies using PET imaging.

Key words Manganese-52 · Antibodies · Bifunctional chelators · Radiolabeling · Trastuzumab · Radiopharmaceuticals

Introduction

PET imaging of large constructs with long biological half-lives leverages the exquisite target specificity of monoclonal antibodies (mAbs) and other agents to assess target expression through tracer quantification in tumors, the targeting of novel drugs and in patient selection, stratification, and monitoring of treatment response [1–7]. Due to the long

✉ Suzanne E. Lapi
lapi@uab.edu

[1] Department of Chemistry, University of Alabama at Birmingham, Birmingham, AL 35205, USA

[2] Department of Radiology, University of Alabama at Birmingham, 1824 6th Ave S, WTI 310F, Birmingham, AL 35294, USA

circulation time of mAbs in the blood, researchers have investigated imaging using long-lived radiometals such as ^{64}Cu ($t_{1/2}$ = 12.7 h), ^{89}Zr ($t_{1/2}$ = 3.3 d), ^{86}Y ($t_{1/2}$ = 14.7 h), ^{111}In ($t_{1/2}$ = 2.8 d) and ^{52}Mn ($t_{1/2}$ = 5.6 d) [8, 9].

Human epidermal growth factor receptor 2 (HER2) is overexpressed in 25–30% of breast cancers (BCa), often indicates an aggressive form of the disease, and is an important therapeutic target [10–17]. Trastuzumab is Food and Drug Administration (FDA) approved mAb that targets HER2 + BCa for treatment with efficacy depending on the HER2 expression levels [18].

^{89}Zr is well-established positron emitter that has been used for HER2 + imaging [5, 9, 18–22]. Since the first evaluation of [^{89}Zr]Zr-trastuzumab in humans by Dijkers et al. [22], several clinical trials using this radiotracer have been reported [23, 24]. [^{89}Zr]Zr-trastuzumab PET/CT imaging of HER2 expression has been used to image metastases in patients with both IHC HER2 positive and negative BCa [22, 24, 25], to predict the efficacy of HER2-targeting antibody–drug-conjugates and support clinical decision making in treatment plans for BCa patients [21, 23].

^{52}Mn is an emerging radiometal for PET imaging at late timepoints after injection due to its long half-life of 5.6 days, low average positron energy (242 keV), and adequate positron decay branching ratio (29.6%). These properties translate to PET images with favorable spatial resolution and motivate the use of ^{52}Mn for imaging of long-lived biologics in addition to ^{64}Cu ($t_{1/2}$ = 12.7 h) and ^{89}Zr ($t_{1/2}$ = 3.3 d) [26–28]. A drawback to ^{52}Mn is the emission of high energy photons (744 (90%), 936 (95%), and 1434 (100%) keV) which leads to additional dose to personnel and may hinder clinical translation [26, 29].

Recent studies have investigated ^{52}Mn labeled mAbs for PET imaging [30]. Graves et al. evaluated [^{52}Mn]Mn-DOTA-TRC105 in 4T1 tumor bearing mice, revealing tumor uptake of 19 ± 3%ID/g and some bone signal 120 h post injection [31]. Ferreira et al. developed YY146, a CD146-targeting mAb [32]. PET imaging of [^{52}Mn]Mn-DOTA-YY146 in tumor bearing mice was used to assess CD146 expression levels in MDA-MB-435, MDA-MB-231 or MCF7 cell lines. MDA-MB-435 xenografts showed highest tumor uptake of 10.2 ± 0.5%ID/g and some bone signal at 120 h postinjection [32]. Csikos et al. synthesized and investigated the properties of [^{52}Mn]Mn-DOTAGA-bevacizumab in KB-3–1 cervix carcinoma tumor-bearing mice through PET/MR imaging and observed high tumor uptake 10 days postinjection [33]. In a more recent study, Toan et al. developed a novel bispyclen-based BFC, BPPA, and used it to conjugate and radiolabel trastuzumab with ^{52}Mn. They further evaluated the biological behavior of [^{52}Mn]Mn-BPPA-trastuzumab in both HER2 + and HER2- mice models out to 10d following injection, using PET/MR imaging [34].

Our group has evaluated the chemistry of commercially available chelators which showed that Oxo-DO3A is a suitable chelator for ^{52}Mn radiolabeling of biomolecules [35]. This work builds on these prior studies and investigates the suitability of three commercially available bifunctional chelators (BFCs) for conjugation with trastuzumab, radiolabeling, and long-term PET imaging of trastuzumab as a model antibody.

Materials and Methods

All chemicals and other reagents were purchased from ThermoFisher Scientific (Hampton, NH) unless otherwise stated. Additional details are provided in the electronic supplementary material (ESM) section.

Production and Quality Control of ^{52}Mn

Production and purification of ^{52}Mn followed previously published procedures [26, 29, 35, 36]. The apparent molar activity (AMA) of the resulting ^{52}Mn was investigated through a chelation assay between ^{52}Mn and serially diluted samples of the chelator DOTA following a published protocol [35].

Conjugation of the BFCs with Trastuzumab

The BFCs: p-SCN-Bn-DOTA, p-SCN-Bn-Oxo-DO3A, and p-SCN-Bn-PCTA (Fig. 1) were conjugated to trastuzumab according to reported studies with some modifications [37–39]. Trastuzumab was reconstituted in water forming a

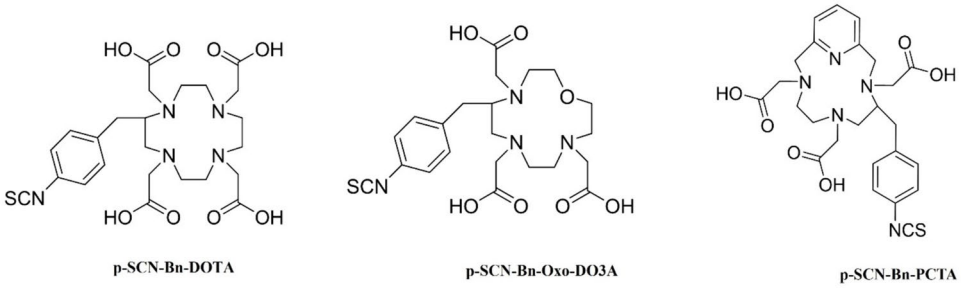

Fig. 1 Selected chelators investigated for conjugation and radiolabeling of trastuzumab with ^{52}Mn.

21 mg/mL stock solution and buffer exchanged into 0.1 M sodium bicarbonate buffer (pH 8.5) using 40 kDa zeba spin desalting columns. The BFCs were dissolved in 0.1 M sodium bicarbonate buffer and a tenfold molar excess of the chelators were incubated with trastuzumab for 1 h at 37 °C [38]. The resulting conjugates were purified, and buffer exchanged into 1 M HEPES (pH 7) using the 40 kDa desalting spin column.

A BCA assay was conducted to quantify the amount of trastuzumab after purification and the immunoconjugates were either stored at 4 °C or used immediately for radiolabeling.

Radiolabeling of BFCs- Trastuzumab with ^{52}Mn

10, 25, 50, and 100 µg of the immunoconjugates were combined with 2.8 MBq (75 µCi) of neutralized [^{52}Mn]$MnCl_2$ with 100 µL of buffer. DOTA-trastuzumab and PCTA-trastuzumab were radiolabeled in 0.1 M ammonium acetate, pH 4 while Oxo-DO3A-trastuzumab was radiolabeled in PBS, pH 7. The reaction mixtures were incubated at 37 °C for 1 h and the radiolabeling yield and purity was assessed by iTLC using a Si-60 iTLC paper developed in 50 mM DTPA (pH 7). Oxo-DO3A-trastuzumab was easily radiolabeled with the highest specific activity of the immunoconjugates and was chosen for further investigation.

Serum Stability

To determine the stability of [^{52}Mn]Mn-Oxo-DO3A-trastuzumab, 30 µL of the radiocomplex was added to 300 µL of mouse serum and incubated at 37 °C for 5 days. At predetermined time points, 50 µL of serum/radiotracer mixture was combined with an equal volume of methanol to precipitate serum proteins and centrifuged at 3700 (revolutions per minute) RPM, 700 (relative centrifugal force) RCF 5 min). The supernatant was analyzed for % intact of the radiotracer using radio iTLC.

In vitro Cell Studies

BT474 (HER2 +) and MDA-MB-468 (HER2-) cell lines were cultured in Gibbco's high glucose Dulbecco' Modified Eagle's Medium (DMEM) supplemented with 10% fetal bovine serum (FBS) and 80 µM gentamicin. 1.8 mM of insulin was also added to the BT474 cell line media. The cells were maintained and grown in humidified incubators at 37 °C with 5% CO_2 atmosphere.

Immunoreactivity

The immunoreactive fraction of [^{52}Mn]Mn-Oxo-DO3A-trastuzumab was determined as described by Lindmo et al. [40]. Experimental details are provided in the ESM section.

Cell Binding

Cell binding assays were performed in BT474 (HER2 +) and MDA-MB-468 (HER2-) cell lines. 5×10^5 cells were seeded in 6-well plates (n = 6) and incubated at 37 °C for 48 h before study. The incubating cell media was removed and 1 mL of fresh media containing 0.5 nM of [^{52}Mn]Mn-Oxo-DO3A-trastuzumab was added to cells which were incubated at 37 °C for 2 h. After incubation, the radioactivity was removed, and the cells were washed in triplicate with ice-cold PBS. 500 µL of 0.2 M NaOH was added to lyse the cells before collection into microcentrifuge-tubes followed by a 500 µL wash of PBS. Associated radioactivity was measured using a Hidex gamma counter. To normalize the counts to the total protein amount, a BCA assay (ThermoFisher Scientific) was performed.

Internalization Assay

Internalization assays were carried out in BT474 (HER2 +) cells following a published procedure with slight modifications [41]. Additional experimental details can be found in the ESM section.

Biodistribution and PET/CT Imaging of [^{52}Mn] Mn-Oxo-DO3A-trastuzumab in Tumor Bearing Mice

All animal studies conducted in this work were performed using a protocol approved by the Institutional Animal Care and Use Committee (IACUC) at the University of Alabama at Birmingham and were compliant with national animal welfare policies and guidelines. The animals were allowed for one week to acclimate prior to any studies.

Mice meant for BT474 (HER2 +) tumors were implanted with a locally made 20 mg cholesterol pellet containing 0.72 mg of β-estradiol to hasten tumor growth as described by Ducharme et al. [15]. 8×10^6 cells of either BT474 (HER2 +) or MDA-MB-468 (HER2-) in complete cell media were subcutaneously injected in the right shoulder. After 6 weeks, tumors were suitable for study ($5 \times 5 \times 5$ mm).

On the study day, [^{52}Mn]Mn-Oxo-DO3A-trastuzumab was synthesized with a specific activity of 16.64 MBq/nmol (450 µCi/nmol). Approximately 0.08 ± 0.01 nmol, 1.29 ± 0.11 MBq (~35 ± 3 µCi) of the immunoconjugate was prepared in 100 µL. Mice (n = 4 per group) were anesthetized with 2.5% isoflurane in oxygen and were injected via the retroorbital sinus. At 3, 5, 7, 10, and 14 d post-injection time points, mice were imaged on a Sofie GNEXT PET/CT small animal scanner (Sofie Biosciences, Dulles, VA, USA). At each time point, 30 min of PET data were acquired

immediately followed by a 3-min CT at 80 kVp for anatomical reference.

At 7 and 14 d post-injection time points, mice were euthanized, and organs were collected, weighed, and radioactivity measured. Radioactivity uptake was calculated as the percent injected dose per gram of tissue (% ID/g). Following reconstruction of the images, regions of interest (ROIs) covering the entire tumor area and corresponding to 3d (VOIs) volumes of interest were hand-drawn using CT images to determine the standardized uptake values (SUVs) using the VivoQuant imaging software.

Statistical Analysis

Data were expressed as mean ± SD. Comparisons were made using GraphPad prism 9 software running student's t-test and 2-way ANOVA utilizing Šídák's multiple comparisons test. P values of less than 0.05 were considered significant.

Results

Production and Quality Control of ^{52}Mn

Approximately 205 ± 19 MBq (5.5 ± 0.5 mCi) ^{52}Mn was produced at the end of a 4 h, 15 µA, and 12.5 MeV on target with an apparent molar activity of ~ 1080.1 ± 81.3 MBq/µmol. ^{54}Mn ($t_{1/2}$ = 312.1 d) was also observed constituting less than 0.4% of the total activity at the end of bombardment.

Conjugation and Radiolabeling

Trastuzumab was successfully conjugated to p-SCN-Bn-DOTA, p-SCN-Bn-Oxo-DO3A, and p-SCN-Bn-PCTA and radiolabeled with ^{52}Mn. Oxo-DO3A-trastuzumab showed the highest RCY of 90 ± 1.5%. The radiolabeling efficiencies of DOTA and PCTA immunoconjugates with similar reaction ratios of 16.64 MBq/nmol all resulted in < 50 ± 2.5% RCY (Fig. 2c).

Oxo-DO3A-trastuzumab was readily radiolabeled with greater than 90% RCY and molar activity of 16.64 MBq/nmol (450 µCi/nmol). This radiotracer was purified resulting in > 98% purity and was chosen for further evaluation.

Serum Stability and Immunoreactivity

[^{52}Mn]Mn-Oxo-DO3A-trastuzumab was stable in mouse serum with > 95% intact for more than 5 days (Fig. 3a) and immunoreactivity fraction was retained at 67 ± 1.2% (Fig. 3b).

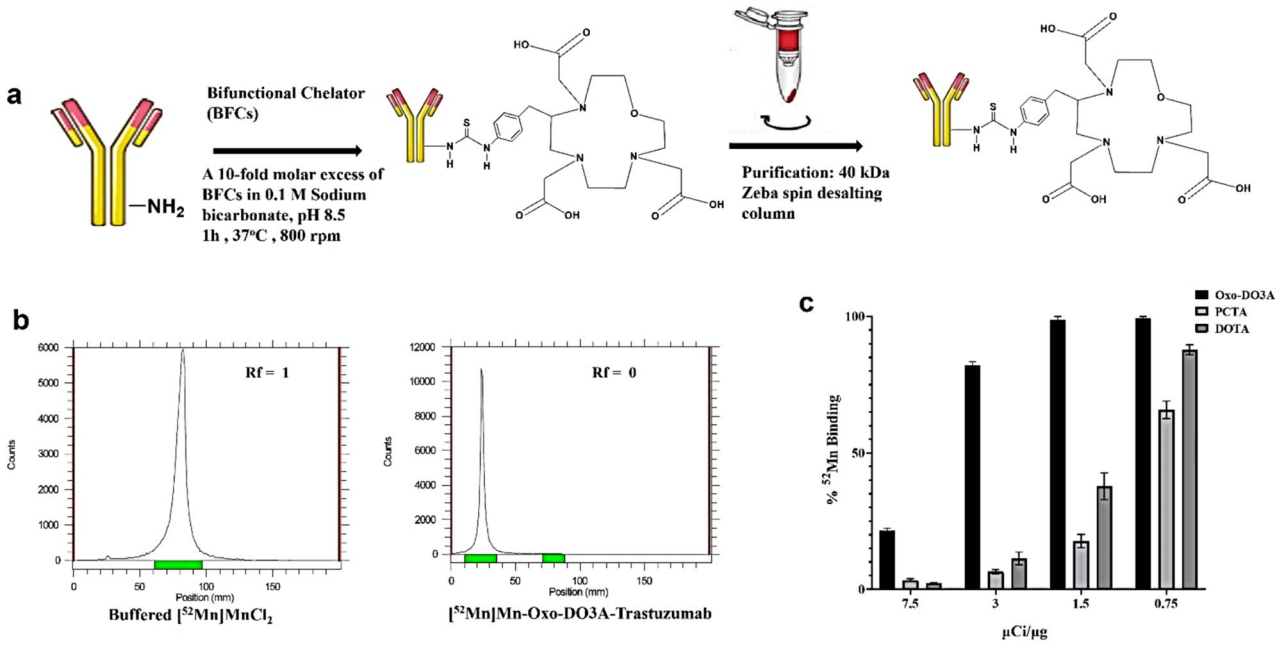

Fig. 2 (**a**) Schematic diagram for steps involved in the conjugation of trastuzumab to different bifunctional chelators. (**b**) Radio TLC chromatograms for free ^{52}Mn which moves with the solvent front and labeled trastuzumab which stays at the origin. (**c**) Comparison of percent labeling efficiency for chelators Oxo-DO3A, PCTA, and DOTA ($n = 3$).

Cell Uptake and Internalization Assay

Cell binding illustrated significantly higher uptake in HER2 positive BT474 (12.51 ± 0.83% /mg) than in HER2 negative MDA-MB-468 (0.85 ± 0.10%/mg $p < 0.0001$) cells (Fig. 3c) after 2 h incubation at 37 °C. The internalized fraction was 10.25 ± 0.5% after 4 h incubation and 41.46 ± 1.68% after 24 h (Fig. 3d).

PET Imaging and Biodistribution of [^{52}Mn] Mn-Oxo-DO3A-trastuzumab

PET images showed uptake and retention of the radiotracer in HER2 + tumors compared to the HER2- tumors (Fig. 4). Tumor uptake was highest at 7d post injection with SUV_{mean} values of 12.79 ± 1.16, *(n = 4)* in HER2 + compared to 0.41 ± 0.08, *(n = 4)* in HER2-; $P < 0.0001$. Gradual clearance of the radiotracer from the kidneys and liver was observed as shown in Tables 1 and 2. Metabolism is primarily hepatic as shown in the PET/CT images. The kinetics of blood pool clearance of the radiotracer is demonstrated by decrease in Heart SUVmean values determined at different time points as shown in Table 1 (HER2 +) and Table 2 (HER2-). Figure 5 shows clearance of the radiotracer in BT474 and MDA-MB-468 tumor models with high uptake and retention of the radiotracer 7 d after injection.

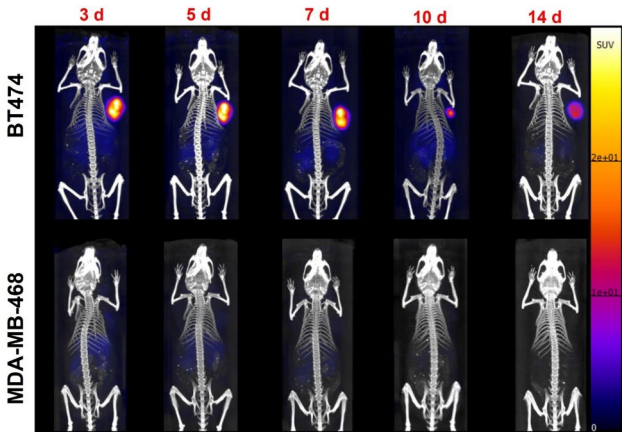

Fig. 4 PET/CT images of [^{52}Mn]Mn-Oxo-DO3A-trastuzumab in BT474 and MDA-MB-468 xenograft models showing images out to 14 d post injection.

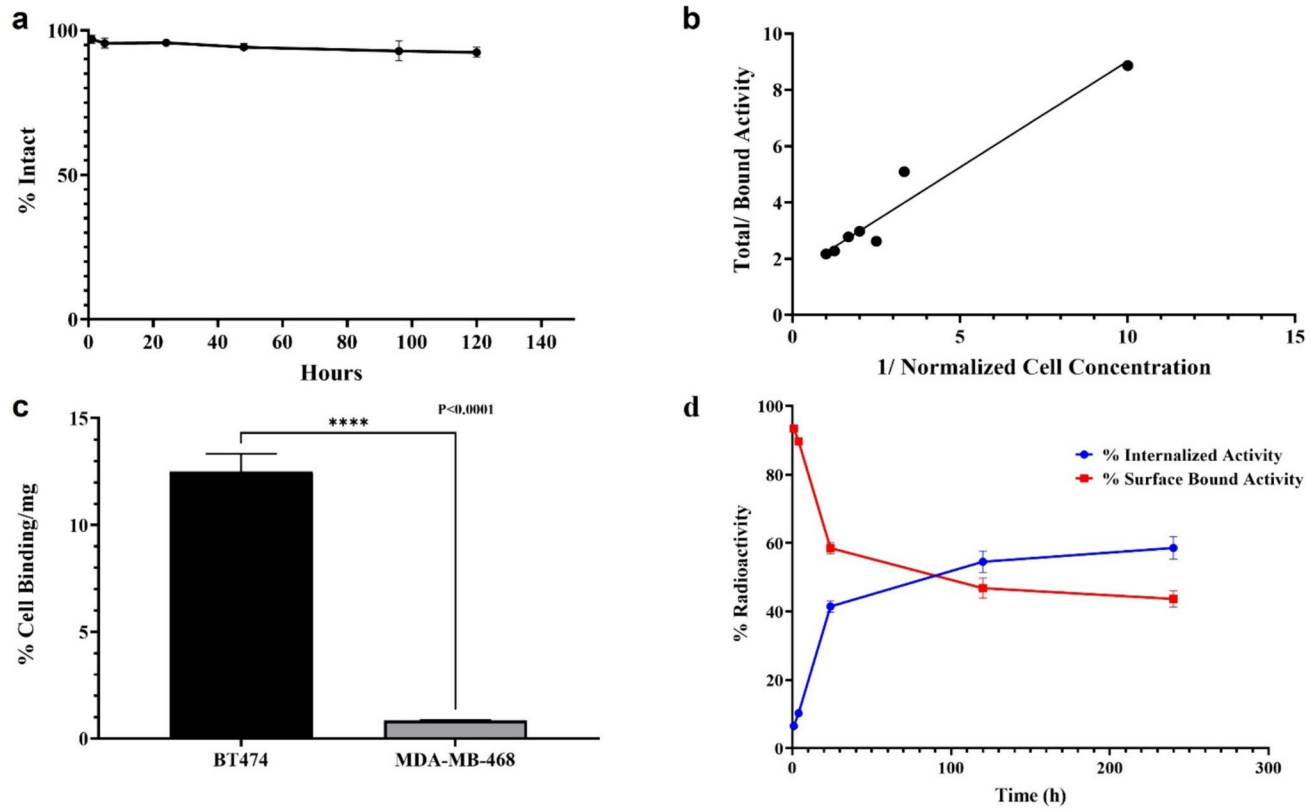

Fig. 3 (**a**) Stability of [^{52}Mn]Mn-Oxo-DO3A-trastuzumab in mouse serum (*n = 3*), (**b**) immunoreactivity fraction of trastuzumab (**c**) Comparison of cell uptake of [^{52}Mn]Mn-Oxo-DO3A-trastuzumab between BT474 and MDA-MB-468 cells (*n = 6*) student unpaired t-test: ****$P < 0.0001$, and (**d**) cell internalization assay of [^{52}Mn]Mn-Oxo-DO3A-trastuzumab in BT474 cells(*n = 6*).

The muscle tissue (along the thigh) was used as background activity. Tumor to muscle ratios using SUV_{mean} values for both HER2 + and HER2- tumors are shown in Fig. 6. The ratios for HER2 + tumors increased steadily and reached the peak at 7d postinjection.

The biodistribution of the radiotracer in mice bearing BT474 and MDA-MB-468 tumors showed similar distribution in all organs except for tumor uptake (Fig. 7). BT474 tumors showed high tumor uptake (38.19 ± 5.91%ID/g,7 d) compared to MDA-MB-468 tumors (2.98 ± 1.13%ID/g, 7 d $p < 0.0001$). The majority of trastuzumab was cleared from the blood by 14 d and notably, femur uptake was very low (0.90 ± 0.15%ID/g, 14 d) (Fig. 7). Table 3 gives a summary of the biodistribution of the radiotracer in both xenograft models.

Discussion

With increasing interest in antibody PET imaging, as well as the progress made in PET imaging techniques to enable the use of very low radiotracer concentrations including higher sensitivity scanners, more positron emitting radiometals are emerging as options alongside ^{64}Cu, ^{89}Zr, and ^{86}Y [9]. For example, Berg et al. reported the feasibility of later time point PET imaging out to 30 d of rhesus monkeys after injection of ^{89}Zr radiotracers using a long bore PET/CT [42].

For late time point imaging, ^{89}Zr- chelates must remain stable to prevent release of ^{89}Zr and subsequent bone uptake. Berg et al. examined the relationship between DFO linker moieties (DFO-Bz-NCS, DFO*-Bz-NCS, DFO-squaramide, and DFO*-squaramide) and stability and found that both DFO*-Bz-NCS and DFO*-squaramide resulted in a lower

Table 1 SUV data of selected organs extracted from PET/CT images for BT474 (HER2 +) and xenograft models at different time points postinjection

Time (day)	Tumor		Heart		Liver		Kidney		Bone	
	HER2 +	HER2-	HER2 +	HER2-	HER2 +	HER2-	HER2 +	HER2-	HER2 +	HER2-
3	4.03 ± 0.94	0.73 ± 0.09	1.78 ± 0.17	0. 67 ± 0.26	1.20 ± 0.64	1.78 ± 0.43	2.11 ± 0.25	1.50 ± 0.03	0.58 ± 0.11	0.27 ± 0.05
5	7.20 ± 1.11	0.58 ± 0.09	0.98 ± 0.16	0.46 ± 0.20	1.50 ± 0.17	0.79 ± 0.30	1.94 ± 0.09	1.38 ± 0.14	0.48 ± 0.03	0.24 ± 0.03
7	12.79 ± 1.16	0.38 ± 0.08	0.76 ± 0.05	0.30 ± 0.08	1.40 ± 0.50	0.50 ± 0.10	2.02 ± 0.16	1.03 ± 0.07	0.42 ± 0.07	0.15 ± 0.02
10	9.20 ± 0.75	0.21 ± 0.03	0.70 ± 0.14	0.13 ± 0.02	1.35 ± 0.20	0.20 ± 0.01	2.13 ± 0.17	0.54 ± 0.11	0.47 ± 0.09	0.10 ± 0.02
14	10.24 ± 1.56	0.10 ± 0.01	0.41 ± 0.17	0.08 ± 0.02	0.85 ± 0.40	0.08 ± 0.01	1.48 ± 0.36	0.28 ± 0.06	0.28 ± 0.07	0.04 ± 0.01

Table 2 SUV data of selected organs extracted from PET/CT images for MDA-MB-468 (HER2-) and xenograft models at different time points postinjection

Time (day)	Tumor	Salivary glands	Heart	Lungs	Liver	Spleen	Pancreas	Kidneys	Muscle	Bone
3	0.76 ± 0.09	0.75 ± 0.20	0.67 ± 0.25	0.63 ± 0.27	1.95 ± 0.81	0.90 ± 0.26	1.15 ± 0.59	1.45 ± 0.13	0.26 ± 0.05	0.31 ± 0.05
5	0.57 ± 0.09	0.66 ± 0.14	0.45 ± 0.20	0.46 ± 0.17	1.08 ± 0.16	0.50 ± 0.18	0.64 ± 0.17	1.30 ± 0.07	0.21 ± 0.03	0.27 ± 0.04
7	0.41 ± 0.08	0.49 ± 0.12	0.29 ± 0.06	0.25 ± 0.09	0.76 ± 0.13	0.34 ± 0.13	0.56 ± 0.13	0.95 ± 0.06	0.13 ± 0.04	0.14 ± 0.05
10	0.20 ± 0.03	0.29 ± 0.10	0.13 ± 0.03	0.13 ± 0.03	0.26 ± 0.04	0.45 ± 0.22	0.23 ± 0.04	0.56 ± 0.10	0.07 ± 0.03	0.10 ± 0.03
14	0.10 ± 0.01	0.13 ± 0.04	0.08 ± 0.03	0.07 ± 0.03	0.11 ± 0.02	0.19 ± 0.06	0.10 ± 0.02	0.26 ± 0.08	0.03 ± 0.01	0.04 ± 0.01

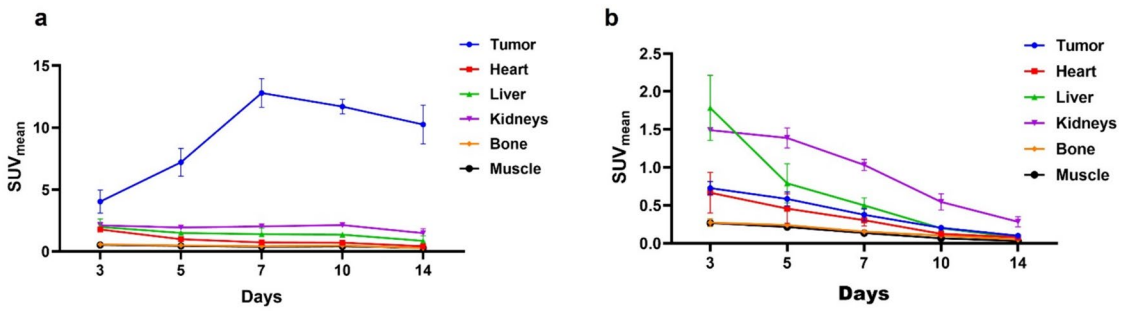

Fig. 5 SUV_{mean} of selected tissues: **a**) HER2 + xenograft models and **b**) HER2- xenograft models.

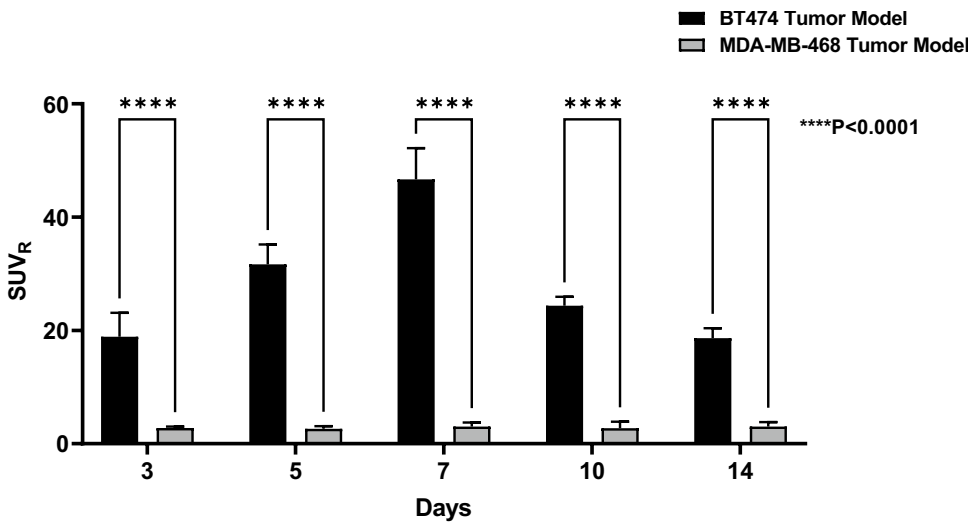

Fig. 6 Tumor to muscle ratios in BT474 and MDA-MB-468 xenograft models at different time points postinjection. 2way ANOVA ****$P < 0.0001$.

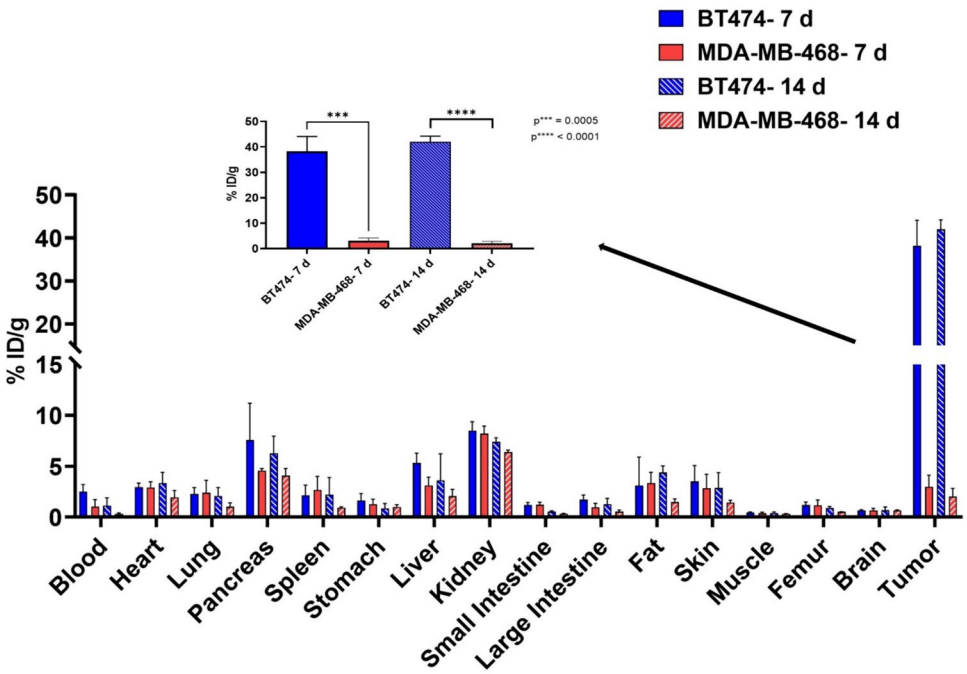

Fig. 7 Biodistribution of [^{52}Mn]Mn-Oxo-DO3A-trastuzumab in BT474 and MDA-MB-468 xenograft models. Student unpaired t-test, (n = 6) ****$P < 0.0001$.

bone uptake [42]. However, while bone uptake has been reported in rodent models, this phenomenon has not been observed in clinical studies [43]. ^{52}Mn is substantially longer lived than ^{64}Cu, or ^{86}Y and may be able to circumvent the enhanced bone uptake observed at long time points with some ^{89}Zr agents [18, 44–46].

Intact antibodies have limitations of low blood clearance and non-specific uptake compared to low molecular weight targeting probes such as affibodies [15, 16]. Váradi et al. synthesized a bifunctional chelator 3,9-PC2ABn^{pCO_2H}, conjugated to a HER2 + targeting affibody and [[^{52}Mn]Mn(3,9-PC2ABn^{pMA})(H2O)]Cys-HER2-affibody, was evaluated *in vivo*. They observed a tumor uptake of SUV_{mean}: 0.63 in HER2 + tumors compared to our reported uptake of SUV_{mean}: 4.03 3d postinjection [47].

The overexpression of HER2 in tumors is associated with aggressive disease, poor prognosis, and shorter overall survival [20]. The effectiveness of trastuzumab therapy depends on HER2 expression [10, 45, 48]. PET imaging with radiolabeled trastuzumab can select patients, monitor treatment response, and determine the optimal dose for a patient [18, 49].

Several preclinical studies and clinical trials involving [^{89}Zr]Zr-trastuzumab have been reported in literature [10, 18, 21, 22, 25, 44, 49–52]. Due to the long residence time in blood of trastuzumab, ^{52}Mn with a longer physical half-life

Table 3 Biodistribution data (% ID/g) of [^{52}Mn]Mn-Oxo-DO3A-trastuzumab in BT474 (HER2+) and MDA-MB-468 (HER2-) xenograft models at 7 d and 14 d postinjection. (mean ± SD) n = 4

Tissue	7 d		14 d	
	HER2+	HER2-	HER2+	HER2-
Blood	2.50 ± 0.69	1.03 ± 0.70	1.13 ± 0.76	0.31 ± 0.12
Heart	2.93 ± 0.42	2.92 ± 0.57	3.36 ± 1.03	1.93 ± 0.70
Lung	2.29 ± 0.62	2.39 ± 1.22	2.09 ± 0.82	1.01 ± 0.41
Pancreas	7.58 ± 3.61	4.57 ± 0.21	6.28 ± 1.67	4.08 ± 0.68
Spleen	2.13 ± 1.01	2.68 ± 1.33	2.21 ± 1.68	0.93 ± 0.09
Stomach	1.63 ± 0.69	1.28 ± 0.48	0.87 ± 0.46	1.00 ± 0.22
Liver	5.30 ± 0.97	3.12 ± 0.81	3.61 ± 2.62	2.06 ± 0.67
Kidney	8.48 ± 0.89	8.21 ± 0.72	7.41 ± 0.39	6.39 ± 0.19
Small intestines	1.21 ± 0.24	1.22 ± 0.23	0.56 ± 0.06	0.33 ± 0.04
Large intestines	1.73 ± 0.45	0.95 ± 0.40	1.26 ± 0.59	0.56 ± 0.14
Fat	3.10 ± 2.78	3.36 ± 1.07	4.38 ± 0.64	1.48 ± 0.32
Skin	3.50 ± 1.58	2.86 ± 1.36	2.86 ± 1.52	1.43 ± 0.23
Muscle	0.47 ± 0.04	0.39 ± 0.09	0.40 ± 0.11	0.33 ± 0.01
Femur	1.18 ± 0.31	1.18 ± 0.51	0.90 ± 0.15	0.52 ± 0.02
Brain	0.67 ± 0.07	0.67 ± 0.19	0.68 ± 0.32	0.67 ± 0.06
Tumor	38.19 ± 5.91	2.98 ± 1.13	42.02 ± 2.16	2.20 ± 0.80

than ^{89}Zr, can also be used to investigate trastuzumab and other antibodies at even later time points.

DOTA with formation constant of LogK_{ML}(19.44) with Mn^{2+} compared to PCTA (16.88), and Oxo-DO3A(13.88) is among the most studied commercial chelator for ^{52}Mn [53]. Biofunctionalized DOTA has been conjugated to different monoclonal antibodies for PET imaging with a significant bone uptake (> 5%ID/g) compared to < 1%ID/g reported herein. The authors attributed this bone uptake to a direct interaction between the bone and the DOTA-bound ^{52}Mn [31–33]. In the current study, BFCs: p-SCN-Bn-DOTA, p-SCN-Bn-Oxo-DO3A, and p-SCN-Bn-PCTA were easily conjugated to trastuzumab following previously published procedures with slight modifications [37–39]. [^{52}Mn]Mn-Oxo-DO3A-trastuzumab was obtained with the highest RCY of 90 ± 1.5% and a molar activity of 16.65 MBq/nmol (450 µCi/nmol) The radiotracer was purified further by a spin desalting column and > 98% purity obtained.

These results were comparable to those reported by Chang et al. who reported radiolabeling trastuzumab with ^{89}Zr with a specific activity of 20.50 MBq/nmol (555 µCi/nmol) and a RCY of 78.4% [18]. Dijkers et al. reported the specific activities and labeling efficiencies of [^{89}Zr]Zr-trastuzumab and [^{111}In]In-trastuzumab as 10.07 MBq/nmol (270 µCi/nmol), 77.6% and 11.72 MBq/nmol (315 µCi/nmol), 89.3% respectively [51].

The radioimmunoconjugate demonstrated greater than 95% intact over a period of 5 days when incubated with mouse serum at 37 °C compared to less than 80% intact of [^{52}Mn]Mn-BPPA-trastuzumab as reported by Toan et al. [34]. The average immunoreactive fraction was determined to be 67 ± 1.2% which was lower compared to > 80% reported with [^{89}Zr]Zr-trastuzumab [18, 49, 51], but was within the acceptance criterion of 65% [49].

In vitro specificity of the radiotracer towards HER2 receptors illustrated a significantly higher % cell uptake in HER2 positive BT474 (12.51 ± 0.83%/mg) than in HER2 negative MDA-MB-468 (0.85 ± 0.10%/mg). Cell binding assays confirmed the HER2 status, however there are reports in the literature that HER2 status can change over time which is a limitation of the study [54].

An internalization assay of [^{52}Mn]Mn-Oxo-DO3A-trastuzumab using the HER2 + BT474 cells demonstrated that 10.26 ± 0.5% of the total activity was internalized after 4 h which later increased to 41.46 ± 1.68% after 24 h incubation at 37 °C. Similar results have been reported with [^{111}In]In-trastuzumab and [^{89}Zr]Zr-trastuzumab utilizing the internalizing properties of trastuzumab antibody and the residualizing nature of ^{111}In and ^{89}Zr radionuclides [9, 37].

In vivo targeting and biodistribution of [^{52}Mn]Mn-Oxo-DO3A-trastuzumab was investigated in nude mice bearing HER2 + BT474 and HER2- MDA-MB-468 tumors. PET images obtained at different time points postinjection: 3, 5, 7, 10, and 14 d showed excellent uptake and retention of the radiotracer with clearance of activity from the liver and the kidney. We hypothesize that the Mn complex stays in Mn^{2+}state but this has not been definitively shown to date.

[^{52}Mn]Mn-Oxo-DO3A-trastuzumab images showed high tumor uptake out to 14 d post injection. Except for tumor uptake, the biodistribution of the [^{52}Mn]Mn-Oxo-DO3A-trastuzumab in both HER2 + and HER2- tumor bearing mice was similar. BT474 tumors showed high tumor uptake (42.02 ± 2.16%ID/g, 14 d) compared to MDA-MB-468 tumors (2.20 ± 0.80%ID/g, 14 d). Literature reports similar biodistribution profiles of [^{111}In]In-trastuzumab and [^{89}Zr]Zr-trastuzumab in mice [18, 37, 50–52]. Chang et al. reported 28.83 ± 1.33% ID/g in HER2 + tumors and 7.91 ± 0.96%ID/g in HER2- tumors 4 d after injection of [^{89}Zr]Zr-trastuzumab. Dijkers et al. reported an uptake of [^{89}Zr]Zr-trastuzumab in HER2 + tumors of 33.4 ± 7.6%ID/g and 7.1 ± 0.7%ID/g in HER2- tumors 6 d postinjection compared to the uptake reported in this study of 34.9 ± 3.0%ID/g in HER2 + and 3.0 ± 1.0%ID/g in HER2- 7 d postinjection [51]. Recently, Toan et al., developed a novel bispyclen-based BFC, BPPA, which was used to radiolabel trastuzumab with ^{52}Mn with a specific activity of 0.085 MBq/µg compared to 0.111 MBq/µg reported herein. *In vivo* investigation of this radiotracer using PET/MR demonstrated high tumor uptake with persistent accumulation of the radiotracer in the liver, kidney, and pancreas where free ^{52}Mn is known to accumulate [34]. [^{52}Mn]Mn-Oxo-DO3A-trastuzumab

demonstrated a slightly higher tumor uptake (SUV_{mean} 12.79 ± 1.16, 7d) compared to [^{52}Mn]Mn-BPPA-trastuzumab (SUV_{mean} 10.08 ± 2.18) reported by Toan et al. [34].

Uptake of ^{89}Zr in bone has been associated with the instability of some ^{89}Zr complexes used in PET imaging. Free ^{52}Mn is known to accumulate in the salivary glands, kidneys, liver, pancreas, and spleen but does not localize in the bone [55]. Biologically, free Mn^{2+} has been shown to exhibit similar behavior to calcium. Observations have been made regarding the diffusion of Mn^{2+} through the voltage dependent calcium channels (VDCCs) and its subsequent accumulation in the pancreas. This feature has been used to track neuronal pathways and monitor β-cell mass as type 1 diabetes progresses [34, 56].

In this study, bone uptake with [^{52}Mn]Mn-Oxo-DO3A-trastuzumab was less than 1%ID/g 7 d post injection compared to > 5%ID/g when [^{89}Zr]Zr-DFO-trastuzumab is used for late time point postinjection [18, 25, 44–46, 57, 58].

Conclusion

In this work, we have demonstrated that the bifunctional chelator Oxo-DO3A is a suitable ^{52}Mn chelator which is readily conjugated, radiolabeled at mild conditions, and illustrated stability over a prolonged duration *in vitro* and *in vivo*. [^{52}Mn]Mn-Oxo-DO3A-trastuzumab was synthesized with > 98% purity and was stable in mouse serum for over 5 days and demonstrated high specificity towards the HER2 receptors through cell binding and internalization assays.

PET imaging of [^{52}Mn]Mn-Oxo-DO3A-trastuzumab in a xenograft model showed high tumor to muscle ratio up to 14 d postinjection in HER2 + tumors. We also observed a low bone uptake (< 1% ID/g) with the ^{52}Mn radiotracer compared to ^{89}Zr labeled trastuzumab (> 5% ID/g). Finally, high uptake of [^{52}Mn]Mn-Oxo-DO3A-trastuzumab in HER2 + (38.2 ± 5.9%ID/g 7d) similar to that of [^{89}Zr]Zr-trastuzumab in HER2 + tumors (33.4 ± 7.6%ID/g 6 d postinjection) can allow the use of ^{52}Mn in a complementary fashion to ^{89}Zr especially in late time point antibody PET imaging to study pharmacokinetics of new antibodies and antibody drug conjugates.

Supplementary Information The online version contains supplementary material available at https://doi.org/10.1007/s11307-024-01948-4.

Author Contribution James M. Omweri: Conceptualization, Data curation, Formal analysis, Investigation, Writing – original draft, Writing – review & editing. Shefali Saini: Formal analysis Investigation, Methodology, Validation, Writing – review & editing. Hailey A. Houson: Formal analysis, Investigation, Methodology, Writing – review & editing. Volkan Tekin: Formal analysis, Investigation, Methodology, Writing – review & editing. Jennifer M. Pyles: Formal analysis, Investigation, Methodology, Writing – review & editing. Candace C. Parker: Formal analysis, Investigation, Visualization, Writing – review & editing. Suzanne E. Lapi: Conceptualization, Formal analysis, Funding acquisition, Investigation, Methodology, Supervision, Writing – review & editing.

Funding This work was funded by the DOE Isotope Program as part of the University Isotope Network through grant DESC0021269 (Principal investigator: Suzanne Lapi). Imaging studies were supported by the Small Animal Imaging Core through O'Neal Cancer Center P30CA013148.

Data Availability The authors declare that the data supporting the findings of this study are available within the paper. Should any new data files be needed in another format they are available from the corresponding author upon reasonable request.

Declarations

Conflict of Interest The authors declare that they have no conflict of interest.

Open Access This article is licensed under a Creative Commons Attribution 4.0 International License, which permits use, sharing, adaptation, distribution and reproduction in any medium or format, as long as you give appropriate credit to the original author(s) and the source, provide a link to the Creative Commons licence, and indicate if changes were made. The images or other third party material in this article are included in the article's Creative Commons licence, unless indicated otherwise in a credit line to the material. If material is not included in the article's Creative Commons licence and your intended use is not permitted by statutory regulation or exceeds the permitted use, you will need to obtain permission directly from the copyright holder. To view a copy of this licence, visit http://creativecommons.org/licenses/by/4.0/.

References

1. Bailly C, Clery PF, Faivre-Chauvet A et al (2016) Immuno-PET for Clinical Theranostic Approaches. Int J Mol Sci 18(1):57
2. Manafi-Farid R, Ataeinia B, Ranjbar S et al (2022) ImmunoPET: Antibody-based PET imaging in solid tumors. Front Med 9:916693
3. Dewulf J, Adhikari K, Vangestel C, Wyngaert TVD, Elvas F (2020) Development of Antibody Immuno-PET/SPECT Radiopharmaceuticals for Imaging of Oncological Disorders-An Update. Cancers 12(7):1868
4. Brown EL, Shmuel S, Mandleywala K et al (2023) Immuno-PET detects antibody-drug potency on coadministration with statins. J Nucl Med 64(10):1638–1646
5. Massicano AVF, Lee S, Crenshaw BK et al (2019) Imaging of HER2 with [(89)Zr]pertuzumab in response to T-DM1 therapy. Cancer Biother Radiopharm 34(4):209–217
6. Mortimer JE, Bading JR, Frankel PH et al (2022) Use of (64) Cu-DOTA-trastuzumab PET to predict response and outcome of patients receiving trastuzumab emtansine for metastatic breast cancer: A pilot study. J Nucl Med 63(8):1145–1148
7. Lau J, Rousseau E, Kwon D, Lin KS, Benard F, Chen X (2020) Insight into the development of PET radiopharmaceuticals for oncology. Cancers 12(5):1312
8. Brasse D, Nonat A (2015) Radiometals: towards a new success story in nuclear imaging? Dalton Trans 44(11):4845–4858
9. Aluicio-Sarduy E, Ellison PA, Barnhart TE, Cai W, Nickles RJ, Engle JW (2018) PET radiometals for antibody labeling. J Labelled Comp Radiopharm 61(9):636–651

10. Slamon DJ, Leyland-Jones B, Shak S et al (2001) Use of chemotherapy plus a monoclonal antibody against HER2 for metastatic breast cancer that overexpresses HER2. N Engl J Med 344(11):783–792
11. Asif HM, Sultana S, Ahmed S, Akhtar N, Tariq M (2016) HER-2 positive breast cancer - a mini-review. Asian Pac J Cancer Prev 17(4):1609–1615
12. Ignatiadis M, Desmedt C, Sotiriou C, de Azambuja E, Piccart M (2009) HER-2 as a target for breast cancer therapy. Clin Cancer Res 15(6):1848–1852
13. Schulz R, Streller F, Scheel AH et al (2014) HER2/ErbB2 activates HSF1 and thereby controls HSP90 clients including MIF in HER2-overexpressing breast cancer. Cell Death Dis 5(1):e980
14. Oh DY, Bang YJ (2020) HER2-targeted therapies - a role beyond breast cancer. Nat Rev Clin Oncol 17(1):33–48
15. Ducharme M, Hall L, Eckenroad W et al (2023) Evaluation of [(89)Zr]Zr-DFO-2Rs15d nanobody for imaging of HER2-positive breast cancer. Mol Pharm 20(9):4629–4639
16. Ge S, Li J, Yu Y et al (2021) Review: Radionuclide molecular imaging targeting HER2 in breast cancer with a focus on molecular probes into clinical trials and small peptides. Molecules 26(21):6482
17. Wang J, Xu B (2019) Targeted therapeutic options and future perspectives for HER2-positive breast cancer. Signal Transduct Target Ther 4(1):34
18. Chang AJ, Desilva R, Jain S, Lears K, Rogers B, Lapi S (2012) 89Zr-radiolabeled trastuzumab imaging in orthotopic and metastatic breast tumors. Pharmaceuticals 5(1):79–93
19. Brandt M, Cardinale J, Aulsebrook ML, Gasser G, Mindt TL (2018) An overview of PET radiochemistry, Part 2: Radiometals. J Nucl Med 59(10):1500–1506
20. Massicano AVF, Marquez-Nostra BV, Lapi SE (2018) Targeting HER2 in nuclear medicine for imaging and therapy. Mol Imaging 17:1536012117745386
21. Gebhart G, Lamberts LE, Wimana Z et al (2016) Molecular imaging as a tool to investigate heterogeneity of advanced HER2-positive breast cancer and to predict patient outcome under trastuzumab emtansine (T-DM1): the ZEPHIR trial. Ann Oncol 27(4):619–624
22. Dijkers EC, Oude Munnink TH, Kosterink JG et al (2010) Biodistribution of 89Zr-trastuzumab and PET imaging of HER2-positive lesions in patients with metastatic breast cancer. Clin Pharmacol Ther 87(5):586–592
23. Bensch F, Brouwers AH, Lub-de Hooge MN et al (2018) (89) Zr-trastuzumab PET supports clinical decision making in breast cancer patients, when HER2 status cannot be determined by standard work up. Eur J Nucl Med Mol Imaging 45(13):2300–2306
24. Ulaner GA, Hyman DM, Lyashchenko SK, Lewis JS, Carrasquillo JA (2017) 89Zr-trastuzumab PET/CT for detection of human epidermal growth factor receptor 2-positive metastases in patients with human epidermal growth factor receptor 2-negative primary breast cancer. Clin Nucl Med 42(12):912–917
25. Ulaner GA, Hyman DM, Ross DS et al (2016) Detection of HER2-positive metastases in patients with HER2-Negative Primary Breast Cancer Using 89Zr-Trastuzumab PET/CT. J Nucl Med 57(10):1523–1528
26. Pyles JM, Massicano AVF, Appiah JP, Bartels JL, Alford A, Lapi SE (2021) Production of (52)Mn using a semi-automated module. Appl Radiat Isot 174:109741
27. Carter LM, Kesner AL, Pratt EC et al (2020) The Impact of Positron Range on PET Resolution, Evaluated with Phantoms and PHITS Monte Carlo Simulations for Conventional and Non-conventional Radionuclides. Mol Imaging Biol 22(1):73–84
28. Le Loirec C, Champion C (2007) Track structure simulation for positron emitters of physical interest. Part II: The case of the radiometals. Nuclear Instruments and Methods in Physics Research Section A: Accelerators, Spectrometers, Detectors and Associated Equipment 582(2):654–664
29. Fonslet J, Tietze S, Jensen AI, Graves SA, Severin GW (2017) Optimized procedures for manganese-52: Production, separation and radiolabeling. Appl Radiat Isot 121:38–43
30. Li M, Wang S, Kong Q, et al (2023) Advances in macrocyclic chelators for positron emission tomography imaging. View 4(5)
31. Graves SA, Hernandez R, Fonslet J et al (2015) Novel Preparation Methods of (52)Mn for ImmunoPET Imaging. Bioconjug Chem 26(10):2118–2124
32. Ferreira CA, Kang L, Li C et al (2021) ImmunoPET of the differential expression of CD146 in breast cancer. Am J Cancer Res 11(4):1586–1599
33. Csikos C, Vágner A, Nagy G, et al (2023) In vivo preclinical assessment of the VEGF targeting potential of the newly synthesized [(52)Mn]Mn-DOTAGA-bevacizumab using experimental cervix carcinoma mouse model. Diagnostics (Basel) 13(2)
34. Toan NM, Vagner A, Nagy G et al (2024) [(52)Mn]Mn-BPPA-Trastuzumab: A Promising HER2-Specific PET Radiotracer. J Med Chem 67(10):8261–8270
35. Omweri JM, Tekin V, Saini S et al (2023) Chelation chemistry of manganese-52 for PET imaging applications. Nucl Med Biol 128–129:108874
36. Pyles JM, Omweri JM, Lapi SE (2023) Natural and enriched Cr target development for production of Manganese-52. Sci Rep 13(1):1167
37. Lub-de Hooge MN, Kosterink JG, Perik PJ et al (2004) Preclinical characterisation of 111In-DTPA-trastuzumab. Br J Pharmacol 143(1):99–106
38. Marquez BV, Ikotun OF, Zheleznyak A et al (2014) Evaluation of (89)Zr-pertuzumab in Breast cancer xenografts. Mol Pharm 11(11):3988–3995
39. Moreau M, Raguin O, Vrigneaud JM, et al (2012) DOTAGA-trastuzumab. A new antibody conjugate targeting HER2/Neu antigen for diagnostic purposes. Bioconjug Chem 23(6):1181–1188
40. Lindmo T, Boven E, Cuttitta F, Fedorko J, Bunn PA (1984) Determination of the immunoreactive function of radiolabeled monoclonal antibodies by linear extrapolation to binding at infinite antigen excess. J Immunol Methods 72(1):77–89
41. Tekin V, Aweda T, Kozgus Guldu O et al (2021) A novel anti-angiogenic radio/photo sensitizer for prostate cancer imaging and therapy: (89)Zr-Pt@TiO(2)-SPHINX, synthesis and in vitro evaluation. Nucl Med Biol 94–95:20–31
42. Berg E, Gill H, Marik J et al (2020) Total-body PET and highly stable chelators together enable meaningful (89)Zr-antibody PET studies up to 30 days after injection. J Nucl Med 61(3):453–460
43. Wuensche TE, Lyashchenko S, van Dongen G, Vugts D (2024) Good practices for (89)Zr radiopharmaceutical production and quality control. EJNMMI Radiopharm Chem 9(1):40
44. Deri MA, Zeglis BM, Francesconi LC, Lewis JS (2013) PET imaging with (8)(9)Zr: from radiochemistry to the clinic. Nucl Med Biol 40(1):3–14
45. van de Watering FC, Rijpkema M, Perk L, Brinkmann U, Oyen WJ, Boerman OC (2014) Zirconium-89 labeled antibodies: A new tool for molecular imaging in cancer patients. Biomed Res Int 2014:203601
46. Abou DS, Ku T, Smith-Jones PM (2011) In vivo biodistribution and accumulation of 89Zr in mice. Nucl Med Biol 38(5):675–681
47. Váradi B, Brezovcsik K, Garda Z et al (2023) Synthesis and characterization of a novel [52Mn]Mn-labelled affibody based radiotracer for HER2+ targeting. Inorg Chem Front 10(16):4734–4745
48. Swain SM, Shastry M, Hamilton E (2023) Targeting HER2-positive breast cancer: advances and future directions. Nat Rev Drug Discov 22(2):101–126
49. Laforest R, Lapi SE, Oyama R et al (2016) [(89)Zr]Trastuzumab: evaluation of radiation dosimetry, safety, and optimal imaging

parameters in women with HER2-positive breast cancer. Mol Imaging Biol 18(6):952–959
50. Kristensen LK, Christensen C, Jensen MM et al (2019) Site-specifically labeled (89)Zr-DFO-trastuzumab improves immunoreactivity and tumor uptake for immuno-PET in a subcutaneous HER2-positive xenograft mouse model. Theranostics 9(15):4409–4420
51. Dijkers EC, Kosterink JG, Rademaker AP et al (2009) Development and characterization of clinical-grade 89Zr-trastuzumab for HER2/neu immunoPET imaging. J Nucl Med 50(6):974–981
52. Holland JP, Caldas-Lopes E, Divilov V et al (2010) Measuring the pharmacodynamic effects of a novel Hsp90 inhibitor on HER2/neu expression in mice using Zr-DFO-trastuzumab. PLoS ONE 5(1):e8859
53. Garda Z, Molnar E, Kalman FK et al (2018) Effect of the nature of donor atoms on the thermodynamic, kinetic and relaxation properties of Mn(II) complexes formed with some trisubstituted 12-membered macrocyclic ligands. Front Chem 6:232
54. Nicolò E, Serafini MS, Munoz-Arcos L et al (2023) Real-time assessment of HER2 status in circulating tumor cells of breast cancer patients: Methods of detection and clinical implications. J Liq Biopsy 8:100117
55. Wooten AL, Aweda TA, Lewis BC, Gross RB, Lapi SE (2017) Biodistribution and PET imaging of pharmacokinetics of manganese in mice using manganese-52. PLoS ONE 12(3):e0174351
56. Boros E, Packard AB (2019) Radioactive transition metals for imaging and therapy. Chem Rev 119(2):870–901
57. Holland JP, Divilov V, Bander NH, Smith-Jones PM, Larson SM, Lewis JS (2010) 89Zr-DFO-J591 for immunoPET of prostate-specific membrane antigen expression in vivo. J Nucl Med 51(8):1293–1300
58. Fischer G, Seibold U, Schirrmacher R, Wangler B, Wangler C (2013) (89)Zr, a radiometal nuclide with high potential for molecular imaging with PET: chemistry, applications and remaining challenges. Molecules 18(6):6469–6490

Publisher's Note Springer Nature remains neutral with regard to jurisdictional claims in published maps and institutional affiliations.